Temporal characteristics of atmospheric ammonia and nitrogen dioxide over China based on emission data, satellite observations and atmospheric transport modeling since 1980

Lei Liu [a], Xiuying Zhang [a, *], Wen Xu [b], Xuejun Liu [b], Yi Li [c], Xuehe Lu [a], Yuehan Zhang [d], Wuting Zhang [a, e]

[a] Jiangsu Provincial Key Laboratory of Geographic Information Science and Technology, International Institute for Earth System Science, Nanjing University, Nanjing 210023, China

[b] College of Resources and Environmental Sciences, Centre for Resources, Environment and Food Security, Key Lab of Plant-Soil Interactions of MOE, China Agricultural University, Beijing 100193, China

[c] Air Quality Division, Arizona Department of Environmental Quality, Phoenix, AZ, 85007, USA

[d] School of Atmospheric Sciences, Nanjing University, Nanjing, China

[e] Jiangsu Center for Collaborative Innovation in Geographical Information Resource Development and Application, Nanjing 210023, China

* Corresponding authors: Xiuying Zhang (lzhxy77@163.com)

Abstract

China is experiencing intense air pollution caused in large part by anthropogenic emissions of reactive nitrogen (Nr). Atmospheric ammonia (NH_3) and nitrogen dioxide (NO_2) are the most important precursors for Nr compounds (including N_2O_5, HNO_3, HONO and particulate NO_3^- and NH_4^+) in the atmosphere. Understanding the changes of NH_3 and NO_2 has important implications for the regulation of anthropogenic Nr emissions, and is a requirement for assessing the consequence of environmental impacts. We conducted the temporal trend analysis of atmospheric NH_3 and NO_2 on a national scale

since 1980 based on emission data (during 1980-2010), satellite observations (for NH_3 since 2008 and for NO_2 since 2005) and atmospheric chemistry transport modeling (during 2008-2015).

Based on the emission data, during 1980-2010, both significant continuous increasing trend of NH_3 and NO_x were observed from REAS (Regional Emission inventory in Asia, for NH_3 0.17 kg N ha^{-1} y^{-2} and for NO_x 0.16 kg N ha^{-1} y^{-2}) and EDGAR (Emissions Database for Global Atmospheric Research, for NH_3 0.24 kg N ha^{-1} y^{-2} and for NO_x 0.17 kg N ha^{-1} y^{-2}) over China. Based on the satellite data and atmospheric chemistry transport modeling named as the Model for Ozone and Related chemical Tracers, version 4 (MOZART-4), the NO_2 columns over China increased significantly from 2005 to 2011 and then decreased significantly from 2011 to 2015; the satellite-retrieved NH_3 columns from 2008 to 2014 increased at a rate of 2.37% y^{-1}. The decrease in NO_2 columns since 2011 may result from more stringent strategies taken to control NO_x emissions during the 12th Five-Year-Plan, while no control policy focused on NH_3 emissions. Our findings provided an overall insight on the temporal trends of both NO_2 and NH_3 since 1980 based on emission data, satellite observations and atmospheric transport modeling. These findings can provide a scientific background for policy-makers that are attempting to control atmospheric pollution in China. Moreover, the multiple datasets used in this study have implications for estimating long-term Nr deposition datasets to assess its impact on soil, forest, water and greenhouse balance.

Keywords: trends, seasonal cycle, ammonia

1. Introduction

Reactive nitrogen (Nr) emissions have increased significantly in China due to anthropogenic activities such as increased combustion of fossil fuels, over-fertilization and high stocking rates of farm animals (Canfield et al., 2010;Galloway et al., 2008;Liu et al., 2013). Elevated Nr in the environment has led to

a series of effects on climate change and ecosystems, e.g. biodiversity loss, stratospheric ozone depletion, air pollution, freshwater eutrophication, the potential alteration of global temperature, drinking water contamination, dead zones in coastal ecosystems and grassland seed bank depletion (Basto et al., 2015;Lan et al., 2015;Shi et al., 2015). Atmospheric reactive N emissions are dominated by nitrogen oxides (NO_x = NO + NO_2) and ammonia (NH_3) (Li et al., 2016a;Galloway et al., 2004). Atmospheric NO_2 and NH_3 are the most important precursors for Nr compounds including N_2O_5, HNO_3, HONO and particulate NO_3^- and NH_4^+ in the atmosphere (Xu et al., 2015;Pan et al., 2012). Therefore, an understanding of both the spatial and temporal patterns of NO_2 and NH_3 is essential for evaluating N-enriched environmental effects, and can provide the scientific background for N pollution mitigation. To investigate the spatial and temporal variations of atmospheric NO_2 and NH_3, ground measurements are acknowledged to be an effective way in monitoring the accurate concentrations of NO_2 and NH_3 (Xu et al., 2015;Pan et al., 2012;Meng et al., 2010). Ground measurements of NO_2 concentrations in China, including about 500 stations in 74 cities, have been monitored and reported to the public since January 2013 (Xie et al., 2015). By the end of 2013, this network was extended with hourly NO_2 concentrations from more than 850 stations in 161 cities. However, there are fewer NH_3 measurements across China than NO_2 measurements. The China Agricultural University has organized a Nationwide Nitrogen Deposition Monitoring Network (NNDMN) since 2010, consisting of 43 monitoring sites covering urban, rural (cropland) and background (coastal, forest and grassland) areas across China (Xu et al., 2015;Liu et al., 2011). Xu et al. (2015) reported the ground NH_3 concentrations throughout China for the first time, providing great potential to understand the ground NH_3 concentrations on a national scale. Other networks include (1) the Chinese Ecosystem Research Network (CERN) which was established in 1988, including 40 field stations (Fu et al., 2010). However, to our knowledge, there are

no detailed reports about ground NH_3 concentrations from CERN on a national scale. (2) Four Chinese cities (Xiamen, Xi-An, Chongqing and Zhuhai) have joined the Acid Deposition Monitoring Network in East Asia (EANET) since 1999. However, only one site (Hongwen, Xiamen) in EANET measured the ground NH_3 concentrations and that data is not continuous. Finally, ground NH_3 concentrations at ten sites in Northern China from 2007 to 2010 have been reported by Pan et al. (2013). All of the above ground measurements provide the potential to understand NH_3 and NO_2 concentrations on a regional scale. However, there is limited information on the spatial and temporal variations of NH_3 and NO_2 in the atmosphere across China. This is due to the limited observation sites and monitoring period, as well as given the uneven distribution of the monitoring sites. Importantly, atmospheric NH_3 and NO_2 monitoring based on ground-based local sites may have limited spatial representativeness of the regional scale as both NH_3 and NO_2 are highly variable in time and space (Clarisse et al., 2009;Wichink Kruit et al., 2012;Boersma et al., 2007).

In order to complement ground-based measurements, satellite observation of NH_3 and NO_2 is a welcome addition for analyzing the recent trends of NH_3 and NO_2 in the atmosphere. Satellite remote sensing offers an opportunity to monitor atmospheric NH_3 and NO_2 with high temporal and spatial resolutions (Warner et al., 2017;Li et al., 2016b). NO_2 was measured by multiple space-based instruments including the Global Ozone Monitoring Experiment (GOME), SCanning Imaging Absorption SpectroMeter for Atmospheric CHartographY (SCIAMACHY), Ozone Monitoring Instrument (OMI) and Global Ozone Monitoring Experiment-2 (GOME-2). The OMI NO_2 provides the best horizontal resolution ($13 \times 24\ km^2$) among instruments in its class and near-global daily coverage (Levelt et al., 2007). OMI observations have been widely applied in environmental-related studies and for the support of emission control policy (Russell et al., 2012;Zhao and Wang, 2009;Castellanos et al.,

2015;Lamsal et al., 2015;Liu et al., 2016a;Foy et al., 2016). First measurements of NH_3 from space were reported over Beijing and San Diego areas with the Tropospheric Emission Spectrometer (TES) (Beer et al., 2008) and in fire plumes in Greece with the Infrared Atmospheric Sounding Interferometer (IASI) (Coheur et al., 2009). The first global map of NH_3 was created from IASI measurements by correlating the observed brightness temperature differences to NH_3 columns using the averaged datasets in 2008 (Clarisse et al., 2009). Shortly after that, many studies focused on developing techniques to gain more reliable NH_3 columns (Whitburn et al., 2016a;Van Damme et al., 2014b), validating the retrieved NH_3 columns using the ground measurements (Van Damme et al., 2014a;Dammers et al., 2016) and comparing the data with the results of the atmospheric chemistry transport models (Van Damme et al., 2014c;Whitburn et al., 2016a), and the estimated NH_3 columns obtained from Fourier transform infrared spectroscopy (FTIR) (Dammers et al., 2016). The retrieval algorithm of obtaining IASI NH_3 columns was based on the method described in Whitburn et al. (2016). Two main steps were performed to derive the NH_3 columns from the satellite measurements. First, derive the spectral hyperspectral range index (HRI) based on each IASI observations (Walker et al., 2011;Van Damme et al., 2014b). Second, convert HRI to NH_3 columns based on a constructed neural network with input parameters including vertical NH_3 profile, satellite viewing angel, surface temperature and so on (Whitburn et al., 2016a). The progresses made on the satellite techniques provide possibility for understanding both the spatial and temporal variations of NH_3 and NO_2 in the atmosphere.

In addition to satellite observations, the emission data are also very important for investigating the temporal trends of NH_3 and NO_2 such as the IIASA inventory (Cofala et al., 2007), EDGAR (Emission Database for Global Atmospheric Research, RAINS-Asia (Regional Air Pollution Information and

Simulation) and Asia REAS (Regional Emission inventory in Asia). REAS is considered as the first inventory by integrating historical, current and future emissions data for Asia based on a consistent methodology (Ohara et al., 2007), and EDGAR is the global emission data with 0.1 by 0.1 grid, which has the highest spatial resolution among different datasets mentioned above. Thus, REAS and EDGAR are used to analyze the historical trends of NH_3 and NO_2 during 1980-2010 in this study. Based on the EDGAR emission data, a widely used atmospheric transport model named as the Model for Ozone and Related chemical Tracers, version 4 (MOZART-4) was also used to model the temporal trend of NH_3 and NO_2 columns during 2008-2015 in comparison with the temporal trends of NH_3 and NO_2 columns measured by satellite instruments.

We aim at getting an overall insight on the temporal trends of both NO_2 and NH_3 since 1980 based on the multiple datasets including the emission data, satellite observations and atmospheric transport modeling. We herein show the Chinese national trend of REAS and EDGAR NH_3 and NO_x emission data during 1980-2010, satellite-retrieved NH_3 during 2008-2015 and NO_2 columns (2005-2015), and atmospheric transport chemistry modeling NH_3 and NO_2 columns (2008-2015). It should be noted here that the satellite NH_3 columns were retrieved from the IASI, and can only be obtained since 2008. It is beneficial to analyze the temporal variations of both NH_3 and NO_2, hence providing a scientific basis for policy makers to reduce N-enriched environmental pollution in China.

2. Materials and methods

2.1. NH_3 and NO_2 Emissions

We examined the emission inventory dataset for Asia REAS (Regional Emission inventory in Asia) with 0.5 °× 0.5 °resolution for the period 1980-2010, and analyzed the temporal trends of NO_x and NH_3 over China. REAS v1.1 is believed to be the first inventory of integrating past, present and future

dataset in Asia based on a consistent methodology. The REAS datasets have been validated by several emissions, and denote agreement with the recent growth status in Chinese emissions (Ohara et al., 2007). We also collected NO_x and NH_3 emission data from EDGAR (Emissions Database for Global Atmospheric Research) v4.3.1, which was developed by the Netherlands Environmental Assessment Agency and European Commission Joint Research Centre (Jgj et al., 2002). The EDGAR emissions are calculated on the basis of a point emissions inventory conducted by the International Energy Agency. EDGAR also has a long time period 1980-2010 with the highest spatial resolution globally (0.1 °×0.1 °) (http://edgar.jrc.ec.europa.eu/overview.php?v=431).

2.2. Satellite observations

IASI is a passive remote-sensing instrument operating in nadir mode and measures the infrared radiation emitted by the Earth's surface and the atmosphere (Clarisse et al., 2009). It covers the entire globe twice a day, crossing the equator at a mean solar local time of 9:30 A.M. and P.M. and has an elliptical footprint of 12 by 12 km up to 20 by 39 km depending on the satellite-viewing angle. In this study we use daytime satellite observations as these are more sensitive to NH_3 and are associated with a large positive thermal contrast and a significant amount of NH_3 (Van Damme et al., 2014b;Whitburn et al., 2016a). The availability of measurements is mainly driven by the cloud coverage as only observations with cloud coverage lower than 25% are processed to be a good compromise between the number of data kept for the analysis and the bias due to the effect of clouds. As the amount of daily data is not always sufficient to obtain meaningful distributions (due to cloud cover or the availability of the temperature profiles from the EUMETSAT operational processing chain) (Van Damme et al., 2014b), it is more appropriate to consider monthly or yearly averages for this trend analysis. We consider IASI observations with a relative error below 100% or an absolute error below 5×10^{15} molec.

154 cm^{-2} for analysis over China. For the error, the filtering depends on the use of the data. Doing this, low
155 columns typical for background conditions with a large relative error but a small absolute error are also
156 taken into account. For other applications, such as comparing with ground measurements, we would
157 recommend to use a threshold of 75% or even 100% relative error. We gained the data upon request
158 from the Atmospheric Spectroscopy Group at Université Libre De Bruxelles
159 (http://www.ulb.ac.be/cpm/atmosphere.html). This data can be gridded on 0.1 ° latitude×0.1 ° longitude
160 (Dammers et al., 2016), 0.25 ° latitude×0.25 ° longitude (Whitburn et al., 2016a) and 0.5 ° latitude×0.5 °
161 longitude (Whitburn et al., 2016b) or even coarser resolutions depending on the usage of the data. For
162 IASI NH_3, we firstly divided China into 0.5 ° latitude×0.5 ° longitude grid. For each grid cell, we
163 calculated the monthly arithmetic mean by averaging the daily values with observations points within
164 the grid cell. Similarly, we calculated the annual arithmetic mean by averaging the daily values with
165 observations points within the grid cell over the whole year.
166 The NO_2 columns are obtained from the OMI instrument on NASA's EOS Aura satellite globally
167 everyday. We used the generated products by the project "Derivation of Ozone Monitoring Instrument
168 tropospheric NO_2 in near-real time" (DOMINO) to analyze the temporal trends of NO_2 columns over
169 China. In DOMINO products, only the observations with a cloud radiance fraction below 0.5 were
170 processed for analysis. The retrieval algorithm is described in detail in the previous work (Boersma et
171 al., 2007) and recent updates can be found in the DOMINO Product Specification Document
172 (http://www.temis.nl/docs/OMI_NO2_HE5_1.0.2.pdf). We used tropospheric NO_2 retrievals from the
173 DOMINO algorithm v2.0. The retrieval quality of NO_2 products is strongly dependent on different
174 aspects of air mass factors, such as radiative transfer calculations, terrain heights and surface albedo.
175 The OMI v2.0 data were mainly improved by more realistic atmospheric profile parameters, and

include more surface albedo and surface pressure reference points than before (Boersma et al., 2011;Boersma et al., 2016). The DOMINO NO_2 datasets are available from http://www.temis.nl/airpollution/no2.html. We should state in particular that we used directly the DOMINO v2.0 products of monthly means from 2005 to 2015 over China for the trend analysis. The DOMINO NO_2 columns were gridded at a resolution of 0.125 °latitude×0.125 °longitude grid globally, which has been widely used for scientific applications (Ma et al., 2013;Ialongo et al., 2016;Castellanos et al., 2015).

To illustrate measurement availability, we presented here some measurement statistics. A total number of cloud-free daytime observations as characterized by the operational IASI processor by year were retrieved in China during 2008-2015 for NH_3 (Fig. 1b). We retrieved more observation numbers after 2010 than those during 2008-2009. In 2010, the update of the improved air temperature profiles, cloud properties products and cloud detection, which are important for calculating the thermal contrast, increased the quality of retrieval (Van Damme et al., 2014b;Van Damme et al., 2014c). In September 2014, there was another update of the air temperature profiles, cloud properties products and cloud detection for calculating the thermal contrast. The version of IASI NH_3 columns used in the present work was based on the method described in Whitburn et al. (2016). We did not use the IASI NH_3 after September 30 in 2014 for the trend analysis because an update of the input meteorological data on 30 September 2014 has caused a substantial increase of the retrieved atmospheric NH_3 columns. For the updates of the IASI-NH_3 data, you can refer to Van Damme et al. (2014b), Van Damme et al. (2014c) and Whitburn et al. (2016). The monthly observation numbers are also presented in Fig. 1a, showing that spring (Mar, Apr and May), summer (Jun, Jul and Aug), autumn (Sep, Oct and Nov) and winter (Dec, Jan and Feb) months represent 29% , 26%, 23% and 21%, respectively. Compared with large

variations of observation numbers for NH_3, the observation numbers for NO_2 varied less by year; winter season had the least, while other seasons varied little.

2.3. Atmospheric transport chemistry model

Atmospheric transport chemistry model is also of central importance in modeling the tropospheric NO_2 and NH_3. We applied a widely used atmospheric global atmospheric transport chemistry model named as the Model for Ozone and Related chemical Tracers, version 4 (MOZART-4) to simulate the tropospheric NO_2 and NH_3 columns during 2008-2015 in accordance with the time period of IASI NH_3 measurements.

The MOZART-4 model is driven by the meteorological data from the NASA Goddard Earth Observing System Model, Version 5 (GEOS-5) at a resolution of 1.9° latitude $\times$ 2.5° longitude spatially. The emission data applied for driving the simulations are based on the updated EDGAR emission inventories. 12 bulk aerosol compounds, 39 photolysis, 85 gas species as well as 157 gas-phase reactions were integrated in MOZART-4. The chemical mechanism on N compounds including the NO_2, NH_3 and aerosols are detailedly integrated to MOZART-4, which is considered to be suitable for tropospheric chemical compositions (Emmons et al., 2010;Pfister et al., 2008;Sahu et al., 2013). The output data used in the current work are temporally varying six hours every day, which were upon request by Louisa Emmons at National Center for Atmospheric Research (NCAR). The monthly means of NO_2 and NH_3 columns were averaged by the daily data, and then used for the trend analysis over China. For more details about MOZART-4, the reader should refer to previous studies (Emmons et al., 2010;Brasseur et al., 1998;Beig and Singh, 2007).

3. Results and discussions

3.1. NH_3 and NO_2 emissions during 1980-2010

We conducted the temporal analysis of NH_3 and NO_x emissions since 1980 based on REAS and EDGAR. Both significant continuous increasing trends of NH_3 and NO_x were observed from REAS (for NH_3 0.17 kg N ha^{-1} y^{-2} and for NO_x 0.16 kg N ha^{-1} y^{-2}) and EDGAR (for NH_3 0.24 kg N ha^{-1} y^{-2} and for NO_x 0.17 kg N ha^{-1} y^{-2}) over China (Fig. 2). We found a relatively consistent increase in NO_x emission from EDGAR and REAS over China, i.e. 0.17 kg N ha^{-1} y^{-2} vs 0.16 kg N ha^{-1} y^{-2}, but inconsistency in the magnitude of NH_3 emissions from EDGAR and REAS over China, i.e. 0.24 kg N ha^{-1} y^{-2} vs 0.17 kg N ha^{-1} y^{-2}. The increase rate in NH_3 emissions over China from EDGAR was much higher than that from REAS, indicating the magnitude of increase trend in NH_3 over China remains a debate, although their thread values (the slope in Fig. 2) of 0.24 kg N ha^{-1} y^{-2} (EDGAR) vs 0.17 kg N ha^{-1} y^{-2} (REAS) both reflected a continuous increasing trend (in this regard they are consistent). It implies that, at least, the NH_3 emissions are indeed increasing during 1980-2010. We also conducted a simple correlation analysis of the NH_3 (Fig. 2a) and NO_x (Fig. 2b) from REAS and EDGAR, showing agreement in the magnitude (slope=1.06) and temporal trend (R^2=0.96) for NO_x, but some inconsistency in the increase rate (slope=1.33) for NH_3.

The discrepancy in the magnitude of NH_3 increase rate from REAS and EDGAR (0.24 kg N ha^{-1} y^{-2} vs 0.17 kg N ha^{-1} y^{-2}) in China since 1980 may be caused by the different emission factors considered for estimating NH_3 emissions. The EDGAR v4.3.1 NH_3 emissions were calculated based on a variety of sectors including agriculture, shipping, waste solid and wastewater, energy for buildings, process emissions during production and application, power industry, oil refineries, transformation industry, combustion for manufacturing, road transportation, railways, pipelines and off-road transport, while the

REAS v1.1 NH_3 emissions focused mainly on the agriculture source (i.e., manure management of livestock and fertilizer application) (Crippa et al., 2015;Ohara et al., 2007). Moreover, the fundamental methodology on estimating the REAS v1.1 NH_3 emissions did not consider the seasonal agricultural variations compared with that of EDGAR v4.3.1 NH_3 emissions (Kurokawa et al., 2013), and the removal efficiency (as a key element to estimate NH_3 emissions) was also reported to be much higher in REAS v1.1 than in EDGAR v4.3.1 (Kurokawa et al., 2013).

A previous study (Liu et al., 2013) summarized published data on the national anthropogenic NH_3 and NO_x emissions with multi-periods in China (Wang et al., 2009;Wang et al., 1997;Streets et al., 2003;Klimont et al., 2001;Sun and Wang, 1997;Olivier et al., 1998;FRCGC, 2007), and also analyzed the temporal pattern of NH_3 emissions. Their results showed that the NH_3 emissions had increased at an annual average rate of 0.32 Tg N y^{-2} (about 0.33 kg N ha^{-1} y^{-2}). The increase rate of NH_3 emissions (0.33 kg N ha^{-1} y^{-2}) by Liu et al. (2013) was double that in REAS (0.17 kg N ha^{-1} y^{-2}), implying that the NH_3 increase rate in China is still an open question, and should be further studied.

3.2. Satellite NH_3 and NO_2 over China in the recent decade

3.2.1. Temporal trends

We referred to the method of a previous study (Russell et al., 2012) to conduct the temporal trend analysis by calculating the average values during cold months (October-March) and warm months (April-September) respectively. We herein concentrated more on the temporal analysis of satellite observations during warm months because of the relatively lower uncertainty in comparison with that during cold months. Fig. 3 shows the temporal trend of NO_2 columns during warm and cold months between 2005 and 2015 as well as monthly average values. From satellite observations, the NO_2 columns over China increased with a slope of 0.063×10^{15} molec. cm^{-2} y^{-1} (4.07% y^{-1}) in warm months

from 2005 to 2011 and then decreased with a slope of -0.072 molec. cm^{-2} in warm months (-3.62% y^{-1}) from 2011 to 2015 (Fig. 3). The decreasing trends were consistent with NO_x emissions since 2011 over China (decreasing from 24.04×10^6 ton in 2011 to 20.78 $\times10^6$ ton in 2014, China Statistical Yearbook, http://www.stats.gov.cn/). During the Chinese 11th Five-Year-Plan (FYP) period (2006-2010), Chinese government undertook a series of strategies to increase energy efficiency and to reduce NO_x emissions, but NO_x emissions were not successfully restrained, which created a big challenge for improving air quality over the country (Xia et al., 2016). During the 12th FYP period (2011-2015), more stringent strategies were implemented to control NO_x emissions, including the application of selective catalytic/non-catalytic reduction (SCR/SNCR) systems in the power sector, staged implementation of tighter vehicle emission standards and a series of standards with aggressive emission limits for power, cement, and the iron and steel industries. These strategies are believed to have helped achieve national targets of NO_x emission abatement (Xia et al., 2016).

However, the satellite-retrieved NH_3 columns increased with a slope of 0.118×10^{15} molec. cm^{-2} y^{-1} (2.37% y^{-1}) in warm months from 2008 to 2014 (Fig. 3). The percent increase rate for NH_3 by year (2.37% y^{-1}) from 2008 to 2014 is lower than that for NO_2 (4.07% y^{-1}) from 2005 to 2011, although the absolute NH_3 increase rate of 0.118×10^{15} molec. cm^{-2} y^{-1} from 2008 to 2014 was higher than absolute NO_2 increase rate of 0.063×10^{15} molec. cm^{-2} y^{-1} from 2005 to 2011. An increase in NH_3 columns from IASI may be due to decreased NH_3 removal leading to a larger fraction maintaining in gaseous state for a long time rather than changing to the condensed phase. Specifically, NH_3 is considered as an important alkaline gas that is abundant in the atmosphere, and is able to neutralize acidic components including HNO_3 and H_2SO_4 through the oxidation of NO_x and SO_2, respectively (Li et al., 2014;Liu et al., 2011;Liu et al., 2017c;Xu et al., 2015). The decreased NH_3 removal to some degree can be

attributed to continuous decreased acidic gases including the NO_2 and SO_2 over China under strong control policy in 12-th FYP, which can largely decrease the fraction of the chemical conversion to $(NH_4)_2SO_4$ and NH_4NO_3 in the atmosphere. Increasing trend in NH_3 columns may be associated with continuous N fertilizer use for guaranteeing increase of crop productions (Erisman et al., 2008). Although there was no strong NH_3 emission control regulation, N fertilizer efficiency should be further improved over China. In 2015, the Ministry of Agriculture formally announced a "Zero Increase Action Plan" for national fertilizer use by 2020, which requires the annual increase in total fertilizer use will be less than 1% from 2015 to 2019, with no further increment from 2020 (Liu et al., 2015).

If the "Zero Increase Action Plan" for N fertilizer can be effective, future NH_3 emissions should be consistent with the current NH_3 emissions. In addition, due to strong emission control of NO_x, the NO_x emissions were believed to decrease significantly from 2011 to 2015. We can reasonably make two major conclusions. First, the atmospheric NO_2, as a key indicator of oxidized N compounds (NO_2, HNO_3 and NO_3^-), decreased since 2011, and will continue to decrease under the current policy. Second, the atmospheric NH_3, as a key indicator of reduced N (NH_3 and particulate NH_4^+), will slightly increase or stay at the current level in the future with the "Zero Increase Action Plan". Thus, due to a decreasing trend of oxidized N (NO_x-N), ammonia N (NH_x-N) should still dominate Nr deposition (oxidized N plus reduced N) in China, and is expected to play a more significant role in Nr deposition. Therefore, monitoring the reduced N on a regional scale is encouraged to assist in enacting effective measures to protect the environments and public health, with respect to air, soil and water quality.

3.2.2. Spatial pattern

High NH_3 columns were found in Beijing, Hebei, Henan, Shandong, Hubei and Jiangsu provinces and in Eastern Sichuan province (Fig. 4a), which were consistent with their high NH_3 emissions due to

306 intensive fertilizer application and livestock (Huang et al., 2012). Guangdong, Guangxi, Hunan and
307 Jiangxi provinces also showed high NH_3 columns, due to high volatilization from paddy fields in these
308 regions, with rice being the dominant crop and contributing the most emissions. High NH_3 columns in
309 southern China are in agreement with the high percent paddy farmland area (Fig. S1a) and the high
310 NH_3 columns in northern China are in agreement with the high percent dry farmland area (Fig. S1b). In
311 addition, the NH_3 emissions from vehicles in urban areas could also contribute to the observed high
312 NH_3 columns. For example, in Beijing, the contribution of vehicles equipped with catalytic converters,
313 particularly since the introduction of three-way-catalysts, to non-agricultural NH_3 emissions has
314 recently been considered and might be the most important factor influencing NH_3 concentrations in
315 urban cities (Meng et al., 2011;Xu et al., 2017). In addition, Xinjiang province also emits remarkable
316 NH_3 emissions related to sheep manure management (Huang et al., 2012;Kang et al., 2016;Zhou et al.,
317 2015;Liu et al., 2017a). The lower NH_3 columns are located mostly in the Tibet Plateau area, where
318 there is a minimal amount of arable land and low use of synthetic nitrogenous fertilizers.
319 NO_2 columns (Fig. 4b) show significantly higher values over vast areas covering North China, East
320 China, and the Sichuan Basin. The NO_2 columns also show high values over the Pearl River Delta, the
321 southern part of Northeast China, and some areas in Northwest China. High NO_2 columns are mostly
322 distributed in populated areas (Fig. S2), where there is a mix of various anthropogenic NO_x sources,
323 such as vehicles and industrial complexes (Wang et al., 2012;Xu et al., 2015;Meng et al., 2010). It
324 should be noted that an enhanced emission intensity from transportation is confirmed since 2005, even
325 with staged implementation of tightened emission standards for on-road vehicles (Wang et al., 2012).
326 For example, NO_x emissions from transportation grew to 30% for the whole country in 2014, and the
327 values reached 44%, 55%, and 33% for Beijing, Shanghai, and Guangdong, respectively (Xia et al.,

2016). Therefore, transportation is believed to play an increasingly important role in regional NO_2 pollution, especially when emissions from stationary sources are gradually controlled through increased penetration of selective catalytic/non-catalytic reduction (SCR/SNCR) systems.

3.2.3. Limitations of satellite observations

It is difficult to gain whole coverage over China based on the daily data for both IASI NH_3 and OMI NO_2. For daily NO_2, the spatial coverage gained by OMI were influenced by cloud radiance fractions, surface albedo, solar zenith angles, row anomaly and so on (Russell et al., 2011;De Smedt et al., 2015). "Row anomaly" issue resulting from the OMI instrumental problem had an impact on approximately half of the rows undergoing unpredictable patterns in cross-track directions relying on latitudes and seasons and prevented obtaining convincing daily product with continuous coverage (Boersma et al., 2011;Boersma et al., 2016). For NH_3, the satellite instruments were strongly dependent on the meteorological conditions such as cloud fractions or the availability of the temperature profiles (Van Damme et al., 2014b;Boersma et al., 2011), and we cannot retrieve the whole coverage based on daily data over China. It will be beneficial to analyze a very local region with enough numbers of observations, but not appropriate to analyze such large coverage over China.

Facing this big challenge, we used the monthly data for the trend analysis over China. The uncertainty of DOMINO v2.0 NO_2 columns has been well documented in Boersma et al. (2011), and the relative error is reported lower than 20-30% in East Asian by an improved altitude-dependent air mass factor look-up table, a more realistic atmospheric profile, an increased number of reference vertical layers and advanced surface albedos (Boersma et al., 2011). The reader is strongly suggested to refer to Boersma et al. (2011) for more details on the uncertainty analysis.

The potential uncertainty of IASI NH_3 columns resulted from IASI observation instruments and

retrieval algorithms. In this paper, the NH_3 datasets were generated based on the recent-updated robust and flexible NH_3 retrieval algorithms, which were designed to overcome some shortcomings of the current algorithms (Whitburn et al., 2016a). The current algorithms were designed firstly to calculate the hyperspectral range index (HRI), a measure for the NH_3 signature strength in the spectrum, and then converted to IASI NH_3 columns by using the thermal contrast (TC) and lookup tables (LUT) of (HRI, TC) pair corresponding to NH_3 columns. The retrieval of HRIs is strongly dependent on the amount of NH_3 and the thermal state of the atmosphere (Whitburn et al., 2016a). The quality of the IASI NH_3 product has been validated by atmospheric chemistry transport models, ground-based and airborne measurements, and NH_3 total columns obtained with ground-based Fourier transform infrared spectroscopy (FTIR). A first validation of the IASI NH_3 using the LOTOS-EUROS model was conducted over Europe, indicating the respective consistency of IASI measurements and model simulations (Van Damme et al., 2014c). A first evaluation of IASI NH_3 dataset using ground-based measurements was made worldwide, presenting consistency with the available ground-based observations and denoting promising results for evaluation by using independent airborne data (Van Damme et al., 2014a). A first validation of of IASI NH_3 dataset using ground-based FTIR derived NH_3 total columns was evaluated, demonstrating a mean relative difference of −32.4±(56.3)%, a correlation r of 0.8 with a slope of 0.73 (Dammers et al., 2016).

3.3. Atmospheric chemistry transport model NO_2 and NH_3 columns since 2008

Satellite NO_2 and NH_3 columns were observed at overpass time as an instantaneous point in a day (at 9:30 A.M. for IASI NH_3 and at 1:45 P.M. for OMI NO_2 local time). These instantaneous satellite observations may not be representative for the temporal trend analysis over China. We further retrieved the monthly variations of NO_2 and NH_3 columns since 2008 from MOZART varying 6 hours every day

372 (00, 06, 12, 18 h). We compared the temporal trend analysis of NO_2 from MOZART at 12 h with that
373 gained from satellite at the overpass time (OMI 1:45 P.M. local time) as well as for NH_3.
374 Fig. 5 shows the NO_2 columns at 12:00 during warm and cold months between 2008 and 2015 from
375 MOZART. The percent increase rate for NO_2 columns at 12:00 during warm months (April-September)
376 between 2008 and 2011 was 4.02% y^{-1} (Fig. 5), which was comparable with that (4.23% y^{-1}) derived
377 from OMI (Fig. 3). During 2011-2015, we found a slightly lower decrease rate (-2.93% y^{-1}) in NO_2
378 columns during warm months at 12:00 from MOZART (Fig. 5) than that (-3.62% y^{-1}) gained from OMI
379 at 13:45 (Fig. 3). The temporal variations of NO_2 columns at 12:00 from MOZART were generally in
380 accord with those from OMI at 13:45 P.M. local time. Fig. 5 also demonstrates the average NO_2
381 columns (averaged at 00, 06, 12 and 18 h) during warm and cold months between 2008 and 2015. We
382 found a close increase rate at 12:00 (4.02%) with that averaged at 00, 06, 12 and 18 h (4.23%) before
383 2011, as well as a similar decrease rate at 12:00 (-2.93%) and the average (-3.07%), implying that the
384 temporal trend analysis at 12:00 vs. that averaged at 00, 06, 12 and 18 h can be considered mostly
385 consistent over China from MOZART.
386 For NH_3, we found the percent increase rate at 12:00 during warm months between 2008 and 2015 was
387 1.30% y^{-1} from MOZART (Fig. 5), which was lower than that (2.37% y^{-1}) from IASI during 2008-2014.
388 The percent increase rate by daily average (at 00, 06, 12 and 18 h) during warm months between 2008
389 and 2015 was 1.36% y^{-1} from MOZART (Fig. 5). In MOZART-4, the alkaline gaseous NH_3 and the
390 acidic gaseous NO_2 (the precursor for HNO_3) and SO_2 are very important precursors for bulk NH_4NO_3
391 and $(NH_4)_2SO_4$ particles, which form the primary system of gas-particle partitioning
392 (NH_3-NH_4^+-NO_x-NO_3^--SO_2-SO_4^{2-}). The chemical shifts between particulate NH_4NO_3 and gaseous NH_3
393 and NO_x are correlated with the abundance of NH_3 and NO_x and meteorological factors. The decreased

abundance of NO_x between 2011 and 2015 may also contribute to an increase in the NH_3 abundance in the gas stage resulting from decreased conversion to particulate NH_4NO_3.

3.4. Implications for estimating long-term Nr deposition datasets and recommendations for future work

We found both the NO_x and NH_3 over China increased continuously from 1980 to 2010 based on emissions data from REAS and EDGAR. In recent years, based on satellite observations, we found an increase of 2.37% y^{-1} in NH_3 columns during 2008-2014. We also found high-level NO_2 columns over China from 2005-2011 (4.07% y^{-1}) but a decrease from 2011 to 2015 (-3.62% y^{-1}). Despite the decline, the NO_2 columns during 2011-2015 were still in high level with an average of 1.87×10^{15} molec. cm^{-2} y^{-1} compared with that (1.65×10^{15} molec. cm^{-2} y^{-1}) during 2005-2010. Notably, these emissions certainly lead to the deposition of atmospheric Nr in form of dry and wet processes into aquatic ecosystems and terrestrial, with implications affecting ecosystem and human health, biological diversity and greenhouse gas balances (Lu et al., 2016). Hence, it is very crucial to estimate Nr deposition with high spatiotemporal resolutions in order to drive ecological models such as the Denitrification-Decomposition (DNDC) model and Integrated BIosphere Simulator (IBIS), to assess its impact on soil, forest, water and greenhouse balance. Here, we call for a long-term dataset of Nr depositions both regionally and globally to investigate how the N emissions affect the environment. Challenge still exits in estimating both the dry (NO_2, HNO_3 particulate NO_3^-, NH_3 and particulate NH_4^+) and wet (NH_4^+ and NO_3^- in precipitation) depositions for a long-term dataset such as since 1980 or earlier possibly due to the complex scheme of N transformations and transportation or limited available data both from emissions, satellites and a limited number of ground measurements.

Satellite observations provide a new perspective of estimating Nr depositions regionally, and have been

used to improve the estimation performance. For example, to improve the modeling performance in dry gaseous NO_2 depositions from GEOS-Chem (Goddard Earth Observing System chemical transport model), Nowlan et al. (2014) applied the OMI NO_2 columns to calibrate the simulated ground NO_2 concentrations, and then estimated the deposition between 2005 and 2007. Our previous work focusing on the dry particulate NO_3^- deposition over China was also based on the OMI NO_2 columns, MOZART simulations and monitored-based sources (Liu et al., 2017b). Geddes et al. (2017) used the satellite NO_2 columns from GOME, GOME-2 and SCIAMACHY instruments to calibrate the NO_x emissions in GEOS-Chem to estimate the NO_x depositions since 1996. The simulations combining the satellite measurements and CTM models to derive Nr depositions (Geddes and Martin, 2017;Nowlan et al., 2014) in recent years will provide relatively accurate datasets (certainly need to be validated and modified by ground measurements).

Despite progress in satellite techniques in recent decades (for NO_2 since 1997 by GOME and for NH_3 since 2008 by IASI), we can hardly tracked studies concerning Nr depositions before 1997 based on satellite observations. Thus, with the help of emissions data such as REAS and EDGAR, we can derive long-term Nr depositions, especially before 1997. Long-term emissions data such as REAS and EDGAR will provide valuable dataset to expand the modeling Nr depositions in recent years. In order to derive the Nr depositions from the emission data, CTMs are frequently used through modeling the wet (simplified as the product of scavenging efficiency and precipitation amount) and dry process (simplified as the inferential method by multiplying the deposition velocity and gaseous or particulate concentrations). However, we still lack a comprehensive dataset of gridded long-term Nr depositions including both the dry (NO_2, HNO_3 particulate NO_3^-, NH_3 and particulate NH_4^+) and wet (NH_4^+ and NO_3^- in precipitation) processes over China, which will be addressed in future work.

Another gap is that, all the above mentioned studies focused on the NO_x depositions and did not derive the NH_y (NH_3 and NH_4^+) depositions over China. Our recent work (Liu et al., 2017a) using IASI NH_3 columns combining the vertical profiles from MOZART benefits our understanding of the ground NH_3 concentrations over China, and the satellite-derived ground NH_3 concentrations were generally in accord with the national measurements from NNDMN. To date, there are still no reports of using the satellite NH_3 columns to derive the temporal and regional NH_y depositions over China, which dominated the total Nr depositions (NO_x plus NH_y) (Liu et al., 2016b;Liu et al., 2013). The gaps of modeling NH_y depositions by applying the satellite observations combining the CTMs simulations require more efforts and further research.

4. Conclusion

Atmospheric ammonia (NH_3) and nitrogen dioxide (NO_2) play an important role in determining air quality, environmental degradation and climate change. The emission data, satellite observations and atmospheric transport modeling have great potential for understanding the temporal variations of atmospheric NH_3 and NO_2 on a regional scale, with high spatial and temporal resolutions. This study analyzed the characteristics of atmospheric NH_3 and NO_2 over China since 1980 based on the multiple datasets. The major findings were as follows:

1. Based on emission data, both significant continuous increasing trend of NH_3 and NO_x were observed from REAS (for NH_3 0.17 kg N ha^{-1} y^{-2} and for NO_x 0.16 kg N ha^{-1} y^{-2}) and EDGAR (for NH_3 0.24 kg N ha^{-1} y^{-2} and for NO_x 0.17 kg N ha^{-1} y^{-2}) over China during 1980-2010.

2. Based on the satellite observations, we found high-level NH_3 columns with the percent increase rate of 2.37% y^{-1} from 2008 to 2014. For NO_2, we found continuous high-level NO_2 columns over China from 2005-2011 but a decrease from 2011 to 2015 (still in high level). The decrease of NO_2 columns

may result from more stringent strategies taken to control NO_x emissions during the 12th Five-Year-Plan, including successful application of SCR/SNCR systems in the power sector, tighter emission standards on vehicles and a series of standards with aggressive emission limits. Increasing trend of NH_3 columns may be due to continuous N fertilizer use for guaranteeing continuous increase of the crop productions. An increase in NH_3 columns may be due to decreased NH_3 removal leading to a larger fraction maintaining in gaseous state for a long time rather than changing to the condensed phase, which may be related with continuous decreased acidic gases including the NO_2 and SO_2 over China under strong control policy in 12-th FYP.

3. Based on MOZART simulations, the temporal variations of NO_2 columns at 12:00 from MOZART were generally in accord with those from OMI at 13:45 P.M. local time. We also found a close increase rate at 12:00 (4.02%) with that averaged at 00, 06, 12 and 18 h (4.23%) before 2011, as well as a similar decrease rate at 12:00 (-2.93%) and the average (-3.07%). For NH_3, we found a lower percent increase rate from MOZART (1.30% y^{-1}) than IASI (2.37% y^{-1}) between 2008 and 2014.

4. The multiple datasets used in the current work have implications for estimating long-term Nr deposition datasets. The simulations combining the satellite measurements and CTM models to derive Nr depositions will provide relatively accurate datasets, and the REAS and EDGAR emissions have potential to expand the modeling Nr depositions to long-term datasets. In particular, modeling NH_y depositions by applying the satellite observations combining the CTMs simulations require more efforts and further research.

Acknowledgements

We acknowledge the free use of tropospheric NO_2 column data from the OMI sensor from www.temis.nl. The NH_3 data have been obtained by the Atmospheric Spectroscopy Group at Universit é

Libre de Bruxelles (ULB) (http://www.ulb.ac.be/cpm/atmosphere.html). S. Whitburn and M. Van Damme are acknowledged for making the data available and for their help in how to use them. We also thank Louisa Emmons from National Center for Atmospheric Research (NCAR) for providing the MOZART output data for the trend analysis. This study is supported by the National Natural Science Foundation of China (No. 41471343, 40425007 and 41101315).

Reference

Basto, S., Thompson, K., Phoenix, G., Sloan, V., Leake, J., and Rees, M.: Long-term nitrogen deposition depletes grassland seed banks, Nature Communication, 6, 1-6, 10.1038/ncomms7185, 2015.

Beer, R., Shephard, M. W., Kulawik, S. S., Clough, S. A., Eldering, A., Bowman, K. W., Sander, S. P., Fisher, B. M., Payne, V. H., Luo, M., Osterman, G. B., and Worden, J. R.: First satellite observations of lower tropospheric ammonia and methanol, Geophysical Research Letters, 35, n/a-n/a, 10.1029/2008GL033642, 2008.

Beig, G., and Singh, V.: Trends in tropical tropospheric column ozone from satellite data and MOZART model, Geophysical Research Letters, 34, 2007.

Boersma, K., Eskes, H., Veefkind, J. P., Brinksma, E., Van Der A, R., Sneep, M., Van Den Oord, G., Levelt, P., Stammes, P., and Gleason, J.: Near-real time retrieval of tropospheric NO2 from OMI, Atmospheric Chemistry and Physics, 7, 2103-2118, 2007.

Boersma, K. F., Eskes, H. J., Dirksen, R. J., van der A, R. J., Veefkind, J. P., Stammes, P., Huijnen, V., Kleipool, Q. L., Sneep, M., Claas, J., Leitão, J., Richter, A., Zhou, Y., and Brunner, D.: An improved tropospheric NO2 column retrieval algorithm for the Ozone Monitoring Instrument, Atmospheric Measurement Techniques, 4, 1905-1928, 10.5194/amt-4-1905-2011, 2011.

Boersma, K. F., Vinken, G. C. M., and Eskes, H. J.: Representativeness errors in comparing chemistry

transport and chemistry climate models with satellite UV–Vis tropospheric column retrievals, Geosci. Model Dev., 9, 875-898, 10.5194/gmd-9-875-2016, 2016.

Brasseur, G., Hauglustaine, D., Walters, S., Rasch, P., Müller, J. F., Granier, C., and Tie, X.: MOZART, a global chemical transport model for ozone and related chemical tracers: 1. Model description, Journal of Geophysical Research: Atmospheres (1984–2012), 103, 28265-28289, 1998.

Canfield, D. E., Glazer, A. N., and Falkowski, P. G.: The Evolution and Future of Earth's Nitrogen Cycle, Science, 330, 192-196, 10.1126/science.1186120, 2010.

Castellanos, P., Boersma, K. F., Torres, O., and De Haan, J. F.: OMI tropospheric NO2 air mass factors over South America: effects of biomass burning aerosols, Atmospheric Measurement Techniques, 8, 2683-2733, 2015.

Clarisse, L., Clerbaux, C., Dentener, F., Hurtmans, D., and Coheur, P.-F.: Global ammonia distribution derived from infrared satellite observations, Nature Geoscience, 2, 479-483, 2009.

Cofala, J., Amann, M., Klimont, Z., Kupiainen, K., and Höglund-Isaksson, L.: Scenarios of global anthropogenic emissions of air pollutants and methane until 2030, Atmospheric Environment, 41, 8486-8499, http://dx.doi.org/10.1016/j.atmosenv.2007.07.010, 2007.

Coheur, P.-F., Clarisse, L., Turquety, S., Hurtmans, D., and Clerbaux, C.: IASI measurements of reactive trace species in biomass burning plumes, Atmospheric Chemistry and Physics, 9, 5655-5667, 2009.

Crippa, M., Janssensmaenhout, G., Dentener, F., Guizzardi, D., Sindelarova, K., Muntean, M., Van Dingenen, R., and Granier, C.: Forty years of improvements in European air quality: the role of EU policy-industry interplay, Atmospheric Chemistry & Physics, 15, 322-337, 2015.

Dammers, E., Palm, M., Van Damme, M., Vigouroux, C., Smale, D., Conway, S., Toon, G. C., Jones,

526 N., Nussbaumer, E., Warneke, T., Petri, C., Clarisse, L., Clerbaux, C., Hermans, C., Lutsch, E., Strong,
527 K., Hannigan, J. W., Nakajima, H., Morino, I., Herrera, B., Stremme, W., Grutter, M., Schaap, M.,
528 Wichink Kruit, R. J., Notholt, J., Coheur, P. F., and Erisman, J. W.: An evaluation of IASI-NH3 with
529 ground-based Fourier transform infrared spectroscopy measurements, Atmos. Chem. Phys., 16,
530 10351-10368, 10.5194/acp-16-10351-2016, 2016.
531 De Smedt, I., Stavrakou, T., Hendrick, F., Danckaert, T., Vlemmix, T., Pinardi, G., Theys, N., Lerot, C.,
532 Gielen, C., and Vigouroux, C.: Diurnal, seasonal and long-term variations of global formaldehyde
533 columns inferred from combined OMI and GOME-2 observations, Atmospheric Chemistry & Physics,
534 15, 12241-12300, 2015.
535 Emmons, L., Walters, S., Hess, P., Lamarque, J.-F., Pfister, G., Fillmore, D., Granier, C., Guenther, A.,
536 Kinnison, D., and Laepple, T.: Description and evaluation of the Model for Ozone and Related
537 chemical Tracers, version 4 (MOZART-4), Geoscientific Model Development, 3, 43-67, 2010.
538 Erisman, J. W., Sutton, M. A., Galloway, J., Klimont, Z., and Winiwarter, W.: How a century of
539 ammonia synthesis changed the world, Nature Geoscience, 1, 636-639, 2008.
540 Foy, B. D., Lu, Z., and Streets, D. G.: Satellite NO2retrievals suggest China has exceeded its
541 NOxreduction goals from the twelfth Five-Year Plan, Scientific Reports, 6, 35912, 2016.
542 Regional Emission Inventory in Asia: http://www.jamstec.go.jp/frsgc/research/d4/emission.htm, 2007.
543 Fu, B., Li, S., Yu, X., Yang, P., Yu, G., Feng, R., and Zhuang, X.: Chinese ecosystem research network:
544 Progress and perspectives, Ecological Complexity, 7, 225-233,
545 http://dx.doi.org/10.1016/j.ecocom.2010.02.007, 2010.
546 Galloway, J. N., Dentener, F. J., Capone, D. G., Boyer, E. W., Howarth, R. W., Seitzinger, S. P., Asner,
547 G. P., Cleveland, C. C., Green, P. A., Holland, E. A., Karl, D. M., Michaels, A. F., Porter, J. H.,

548 Townsend, A. R., and Vöosmarty, C. J.: Nitrogen Cycles: Past, Present, and Future, Biogeochemistry,
549 70, 153-226, 10.1007/s10533-004-0370-0, 2004.
550 Galloway, J. N., Townsend, A. R., Erisman, J. W., Bekunda, M., Cai, Z., Freney, J. R., Martinelli, L. A.,
551 Seitzinger, S. P., and Sutton, M. A.: Transformation of the Nitrogen Cycle: Recent Trends, Questions,
552 and Potential Solutions, Science, 320, 889-892, 10.1126/science.1136674, 2008.
553 Geddes, J. A., and Martin, R. V.: Global deposition of total reactive nitrogen oxides from 1996 to 2014
554 constrained with satellite observations of NO2 columns, Atmos. Chem. Phys. Discuss., 2017, 1-44,
555 10.5194/acp-2016-1100, 2017.
556 Huang, X., Song, Y., Li, M., Li, J., Huo, Q., Cai, X., Zhu, T., Hu, M., and Zhang, H.: A high resolution
557 ammonia emission inventory in China, Global Biogeochemical Cycles, 26, 1-14, 2012.
558 Ialongo, I., Herman, J., Krotkov, N., Lamsal, L., Boersma, K. F., Hovila, J., and Tamminen, J.:
559 Comparison of OMI NO2 observations and their seasonal and weekly cycles with ground-based
560 measurements in Helsinki, 1-13, 2016.
561 Jgj, O., Jjm, B., Jahw, P., Bakker, J., Ajh, V., and Jpj, B.: Applications of EDGAR Emission Database
562 for Global Atmospheric Research, Rijksinstituut Voor Volksgezondheid En Milieu Rivm, 2002.
563 Kang, Y., Liu, M., Song, Y., Huang, X., Yao, H., Cai, X., Zhang, H., Kang, L., Liu, X., Yan, X., He, H.,
564 Zhang, Q., Shao, M., and Zhu, T.: High-resolution ammonia emissions inventories in China from 1980
565 to 2012, Atmos. Chem. Phys., 16, 2043-2058, 10.5194/acp-16-2043-2016, 2016.
566 Klimont, Z., Cofala, J., Schöpp, W., Amann, M., Streets, D. G., Ichikawa, Y., and Fujita, S.: Projections
567 of SO2, NOx, NH3 and VOC Emissions in East Asia Up to 2030, Water, Air, & Soil Pollution, 130,
568 193-198, 2001.
569 Kurokawa, J., Ohara, T., Morikawa, T., and Hanayama, S.: Emissions of air pollutants and greenhouse

570 gases over Asian regions during 2000–2008: Regional Emission inventory in ASia (REAS) version 2,
571 Atmospheric Chemistry & Physics, 13, 10049-10123, 2013.
572 Lamsal, L. N., Duncan, B. N., Yoshida, Y., Krotkov, N. A., Pickering, K. E., Streets, D. G., and Lu, Z.:
573 U.S. NO2 trends (2005–2013): EPA Air Quality System (AQS) data versus improved observations from
574 the Ozone Monitoring Instrument (OMI), Atmospheric Environment, 110, 130-143,
575 http://dx.doi.org/10.1016/j.atmosenv.2015.03.055, 2015.
576 Lan, Z., Jenerette, G. D., Zhan, S., Li, W., Zheng, S., and Bai, Y.: Testing the scaling effects and
577 mechanisms of N-induced biodiversity loss: evidence from a decade-long grassland experiment,
578 Journal of Ecology, 103, 750-760, 10.1111/1365-2745.12395, 2015.
579 Levelt, P., Stammes, P., Gleason, J., and Bucsela, E.: Near-real time retrieval of tropospheric NO2 from
580 OMI, Atmospheric Chemistry and Physics, 7, 2103-2118, 2007.
581 Li, Y., Schwandner, F. M., Sewell, H. J., Zivkovich, A., Tigges, M., Raja, S., Holcomb, S., Molenar, J.
582 V., Sherman, L., and Archuleta, C.: Observations of ammonia, nitric acid, and fine particles in a rural
583 gas production region, Atmospheric Environment, 83, 80-89, 2014.
584 Li, Y., Schichtel, B. A., Walker, J. T., Schwede, D. B., Chen, X., Lehmann, C. M., Puchalski, M. A.,
585 Gay, D. A., and Collett, J. L.: Increasing importance of deposition of reduced nitrogen in the United
586 States, Proceedings of the National Academy of Sciences, 113, 5874-5879, 2016a.
587 Li, Y., Thompson, T. M., Van Damme, M., Chen, X., Benedict, K. B., Shao, Y., Day, D., Boris, A.,
588 Sullivan, A. P., Ham, J., Whitburn, S., Clarisse, L., Coheur, P. F., and Collett Jr, J. L.: Temporal and
589 Spatial Variability of Ammonia in Urban and Agricultural Regions of Northern Colorado, United States,
590 Atmos. Chem. Phys. Discuss., 2016, 1-50, 10.5194/acp-2016-1008, 2016b.
591 Liu, F., Zhang, Q., Ronald, J. v. d. A., Zheng, B., Tong, D., Yan, L., Zheng, Y., and He, K.: Recent

592 reduction in NO x emissions over China: synthesis of satellite observations and emission inventories,
593 Environmental Research Letters, 11, 114002, 2016a.
594 Liu, L., Zhang, X., Wang, S., Lu, X., and Ouyang, X.: A Review of Spatial Variation of Inorganic
595 Nitrogen (N) Wet Deposition in China, PloS one, 11, e0146051, 2016b.
596 Liu, L., Zhang, X., Xu, W., Liu, X., Lu, X., Wang, S., Zhang, W., and Zhao, L.: Ground Ammonia
597 Concentrations over China Derived from Satellite and Atmospheric Transport Modeling, Remote
598 Sensing, 9, 467, 2017a.
599 Liu, L., Zhang, X., Zhang, Y., Xu, W., Liu, X., Zhang, X., Feng, J., Chen, X., Zhang, Y., Lu, X., Wang,
600 S., Zhang, W., and Zhao, L.: Dry Particulate Nitrate Deposition in China, Environmental Science &
601 Technology, 10.1021/acs.est.7b00898, 2017b.
602 Liu, X., Duan, L., Mo, J., Du, E., Shen, J., Lu, X., Zhang, Y., Zhou, X., He, C., and Zhang, F.: Nitrogen
603 deposition and its ecological impact in China: An overview, Environmental Pollution, 159, 2251-2264,
604 http://dx.doi.org/10.1016/j.envpol.2010.08.002, 2011.
605 Liu, X., Zhang, Y., Han, W., Tang, A., Shen, J., Cui, Z., Vitousek, P., Erisman, J. W., Goulding, K., and
606 Christie, P.: Enhanced nitrogen deposition over China, Nature, 494, 459-462, 2013.
607 Liu, X., Vitousek, P., Chang, Y., Zhang, W., Matson, P., and Zhang, F.: Evidence for a Historic Change
608 Occurring in China, Environmental Science & Technology, 50, 505-506, 2015.
609 Liu, X., Xu, W., Duan, L., Du, E., Pan, Y., Lu, X., Zhang, L., Wu, Z., Wang, X., and Zhang, Y.: Erratum
610 to: Atmospheric Nitrogen Emission, Deposition, and Air Quality Impacts in China: an Overview,
611 Current Pollution Reports, 1-1, 2017c.
612 Lu, X., Jiang, H., Liu, J., Zhang, X., Jin, J., Zhu, Q., Zhang, Z., and Peng, C.: Simulated effects of
613 nitrogen saturation on the global carbon budget using the IBIS model, Scientific Reports, 6, 39173,

614 10.1038/srep39173, 2016.

615 Ma, J. Z., Beirle, S., Jin, J. L., Shaiganfar, R., Yan, P., and Wagner, T.: Tropospheric NO2 vertical
616 column densities over Beijing: results of the first three years of ground-based MAX-DOAS
617 measurements (2008–2011) and satellite validation, Atmospheric Chemistry & Physics, 13, 1547-1567,
618 2013.

619 Meng, Z.-Y., Xu, X.-B., Wang, T., Zhang, X.-Y., Yu, X.-L., Wang, S.-F., Lin, W.-L., Chen, Y.-Z., Jiang,
620 Y.-A., and An, X.-Q.: Ambient sulfur dioxide, nitrogen dioxide, and ammonia at ten background and
621 rural sites in China during 2007–2008, Atmospheric Environment, 44, 2625-2631,
622 http://dx.doi.org/10.1016/j.atmosenv.2010.04.008, 2010.

623 Meng, Z., Lin, W., Jiang, X., Yan, P., Wang, Y., Zhang, Y., Jia, X., and Yu, X.: Characteristics of
624 atmospheric ammonia over Beijing, China, Atmospheric Chemistry and Physics, 11, 6139-6151, 2011.

625 Nowlan, C., Martin, R., Philip, S., Lamsal, L., Krotkov, N., Marais, E., Wang, S., and Zhang, Q.:
626 Global dry deposition of nitrogen dioxide and sulfur dioxide inferred from space‐based measurements,
627 Global Biogeochemical Cycles, 28, 1025-1043, 2014.

628 Ohara, T., Akimoto, H., Kurokawa, J., Horii, N., Yamaji, K., Yan, X., and Hayasaka, T.: An Asian
629 emission inventory of anthropogenic emission sources for the period 1980–2020, Atmos. Chem.
630 Phys., 7, 4419-4444, 10.5194/acp-7-4419-2007, 2007.

631 Olivier, J. G. J., Bouwman, A. F., Hoek, K. W. V. D., and Berdowski, J. J. M.: Global air emission
632 inventories for anthropogenic sources of NO x , NH 3 and N 2 O in 1990, Environmental Pollution,
633 102, 135-148, 1998.

634 Pan, Y., Wang, Y., Tang, G., and Wu, D.: Wet and dry deposition of atmospheric nitrogen at ten sites in
635 Northern China, Atmospheric Chemistry and Physics, 12, 6515-6535, 2012.

636 Pfister, G., Emmons, L., Hess, P., Lamarque, J. F., Orlando, J., Walters, S., Guenther, A., Palmer, P., and
637 Lawrence, P.: Contribution of isoprene to chemical budgets: A model tracer study with the NCAR CTM
638 MOZART‐4, Journal of Geophysical Research: Atmospheres (1984–2012), 113, 2008.
639 Russell, A., Valin, L., and Cohen, R.: Trends in OMI NO 2 observations over the United States: effects
640 of emission control technology and the economic recession, Atmospheric Chemistry and Physics, 12,
641 12197-12209, 2012.
642 Russell, A. R., Perring, A. E., Valin, L. C., and Bucsela, E. J.: A high spatial resolution retrieval of NO
643 2 column densities from OMI: method and evaluation, Atmospheric Chemistry & Physics, 11,
644 12411-12440, 2011.
645 Sahu, L., Sheel, V., Kajino, M., Gunthe, S. S., Thouret, V., Nedelec, P., and Smit, H. G.: Characteristics
646 of tropospheric ozone variability over an urban site in Southeast Asia: A study based on MOZAIC and
647 MOZART vertical profiles, Journal of Geophysical Research: Atmospheres, 118, 8729-8747, 2013.
648 Shi, Y., Cui, S., Ju, X., Cai, Z., and Zhu, Y.-G.: Impacts of reactive nitrogen on climate change in China,
649 Scientific Reports, 5, 8118, 10.1038/srep08118
650 http://www.nature.com/articles/srep08118#supplementary-information, 2015.
651 Streets, D. G., Bond, T. C., Carmichael, G. R., Fernandes, S. D., He, D., Klimont, Z., Nelson, S. M.,
652 Tsai, N. Y., and Wang, M. Q.: An inventory of gaseous and primary aerosol emissions in Asia in the
653 year 2000, Journal of Geophysical Research Atmospheres, 108, GTE 30-31, 2003.
654 Sun, Q., and Wang, M.: Ammonia Emission and Concentration in the Atmosphere over China, Scientia
655 Atmospherica Sinica, 1997.
656 Van Damme, M., Clarisse, L., Dammers, E., Liu, X., Nowak, J., Clerbaux, C., Flechard, C.,
657 Galy-Lacaux, C., Xu, W., and Neuman, J.: Towards validation of ammonia (NH3) measurements from

the IASI satellite, Atmospheric Measurement Techniques, 7, 12125-12172, 2014a.

Van Damme, M., Clarisse, L., Heald, C., Hurtmans, D., Ngadi, Y., Clerbaux, C., Dolman, A., Erisman, J. W., and Coheur, P.-F.: Global distributions, time series and error characterization of atmospheric ammonia (NH3) from IASI satellite observations, Atmospheric Chemistry and Physics, 14, 2905-2922, 2014b.

Van Damme, M., Wichink Kruit, R., Schaap, M., Clarisse, L., Clerbaux, C., Coheur, P. F., Dammers, E., Dolman, A., and Erisman, J.: Evaluating 4 years of atmospheric ammonia (NH3) over Europe using IASI satellite observations and LOTOS‐EUROS model results, Journal of Geophysical Research: Atmospheres, 119, 9549-9566, 2014c.

Walker, J. C., Dudhia, A., and Carboni, E.: An effective method for the detection of trace species demonstrated using the MetOp Infrared Atmospheric Sounding Interferometer, Atmos. Meas. Tech., 4, 1567-1580, 10.5194/amt-4-1567-2011, 2011.

Wang, S., Zhang, Q., Streets, D., He, K., Martin, R., Lamsal, L., Chen, D., Lei, Y., and Lu, Z.: Growth in NO x emissions from power plants in China: bottom-up estimates and satellite observations, Atmospheric Chemistry and Physics, 12, 4429-4447, 2012.

Wang, S. W., Liao, J. H., Yu-Ting, H. U., and Yan, X. Y.: A Preliminary Inventory of NH_3-N Emission and Its Temporal and Spatial Distribution of China, Journal of Agro-Environment Science, 2009.

Wang, W. X., Lu, X. F., Pang, Y. B., Tang, D. G., and Zhang, W. H.: Geographical distribution of NH3 emission intensities in China, Actaentiae Circumstantiae, 1997.

Warner, J. X., Dickerson, R. R., Wei, Z., Strow, L. L., Wang, Y., and Liang, Q.: Increased atmospheric ammonia over the world's major agricultural areas detected from space, Geophysical Research Letters, n/a-n/a, 10.1002/2016GL072305, 2017.

680 Whitburn, S., Van Damme, M., Clarisse, L., Bauduin, S., Heald, C. L., Hadji-Lazaro, J., Hurtmans, D.,
681 Zondlo, M. A., Clerbaux, C., and Coheur, P. F.: A flexible and robust neural network IASI-NH3
682 retrieval algorithm, Journal of Geophysical Research: Atmospheres, 121, 6581-6599,
683 10.1002/2016JD024828, 2016a.
684 Whitburn, S., Van Damme, M., Clarisse, L., Turquety, S., Clerbaux, C., and Coheur, P. F.: Doubling of
685 annual ammonia emissions from the peat fires in Indonesia during the 2015 El Niño, Geophysical
686 Research Letters, 43, 11,007-011,014, 10.1002/2016GL070620, 2016b.
687 Wichink Kruit, R. J., Schaap, M., Sauter, F. J., van Zanten, M. C., and van Pul, W. A. J.: Modeling the
688 distribution of ammonia across Europe including bi-directional surface–atmosphere exchange,
689 Biogeosciences, 9, 5261-5277, 10.5194/bg-9-5261-2012, 2012.
690 Xia, Y., Zhao, Y., and Nielsen, C. P.: Benefits of China's efforts in gaseous pollutant control indicated
691 by the bottom-up emissions and satellite observations 2000–2014, Atmospheric Environment, 136,
692 43-53, http://dx.doi.org/10.1016/j.atmosenv.2016.04.013, 2016.
693 Xie, Y., Zhao, B., Zhang, L., and Luo, R.: Spatiotemporal variations of PM2.5 and PM10
694 concentrations between 31 Chinese cities and their relationships with SO2, NO2, CO and O3,
695 Particuology, 20, 141-149, http://dx.doi.org/10.1016/j.partic.2015.01.003, 2015.
696 Xu, W., Luo, X. S., Pan, Y. P., Zhang, L., Tang, A. H., Shen, J. L., Zhang, Y., Li, K. H., Wu, Q. H., Yang,
697 D. W., Zhang, Y. Y., Xue, J., Li, W. Q., Li, Q. Q., Tang, L., Lv, S. H., Liang, T., Tong, Y. A., Liu, P.,
698 Zhang, Q., Xiong, Z. Q., Shi, X. J., Wu, L. H., Shi, W. Q., Tian, K., Zhong, X. H., Shi, K., Tang, Q. Y.,
699 Zhang, L. J., Huang, J. L., He, C. E., Kuang, F. H., Zhu, B., Liu, H., Jin, X., Xin, Y. J., SHi, X. K., Du,
700 E. Z., Dore, A. J., Tang, S., Collett Jr, J. L., Goulding, K., Sun, Y. X., Ren, J., Zhang, F. S., and Liu, X.
701 J.: Quantifying atmospheric nitrogen deposition through a nationwide monitoring network across China,

Atmospheric Chemistry and Physics, 15, 12345-12360, 2015.

Xu, W., Song, W., Zhang, Y., Liu, X., Zhang, L., Zhao, Y., Liu, D., Tang, A., Yang, D., and Wang, D.: Air quality improvement in a megacity: implications from 2015 Beijing Parade Blue pollution control actions, Atmospheric Chemistry and Physics, 17, 31-46, 2017.

Zhao, C., and Wang, Y.: Assimilated inversion of NOx emissions over east Asia using OMI NO2 column measurements, Geophysical Research Letters, 36, 1-5, 2009.

Zhou, Y., Shuiyuan, C., Lang, J., Chen, D., Zhao, B., Liu, C., Xu, R., and Li, T.: A comprehensive ammonia emission inventory with high-resolution and its evaluation in the Beijing–Tianjin–Hebei (BTH) region, China, Atmospheric Environment, 106, 305-317, http://dx.doi.org/10.1016/j.atmosenv.2015.01.069, 2015.

Figures

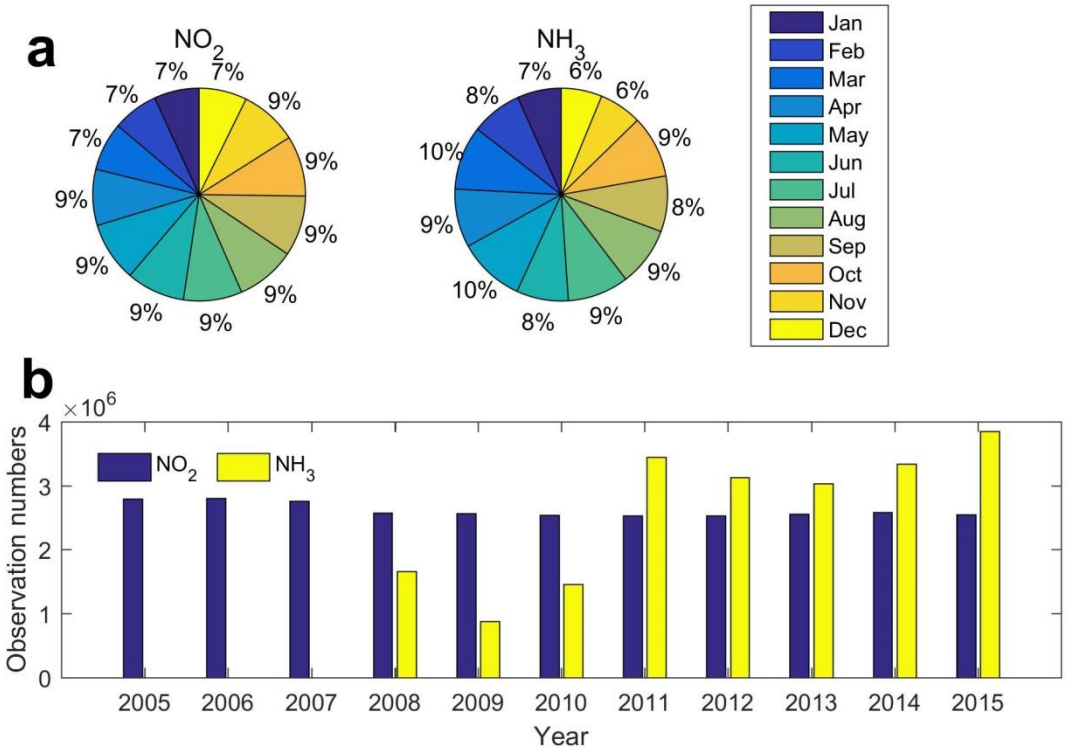

Fig. 1. The satellite-derived observation numbers for NO_2 and NH_3. (a) denotes the percentages of observations in each month in 2010 for NO_2 and in 2015 for NH_3 and (b) represents the total observation numbers for NO_2 and NH_3 over China. Notably, the NO_2 observation numbers were gained from DOMINO products with a cloud radiance fraction below 0.5, while the IASI observations with a relative error below 100% or an absolute error below 5×10^{15} molec. cm^{-2} were processed for analysis over China.

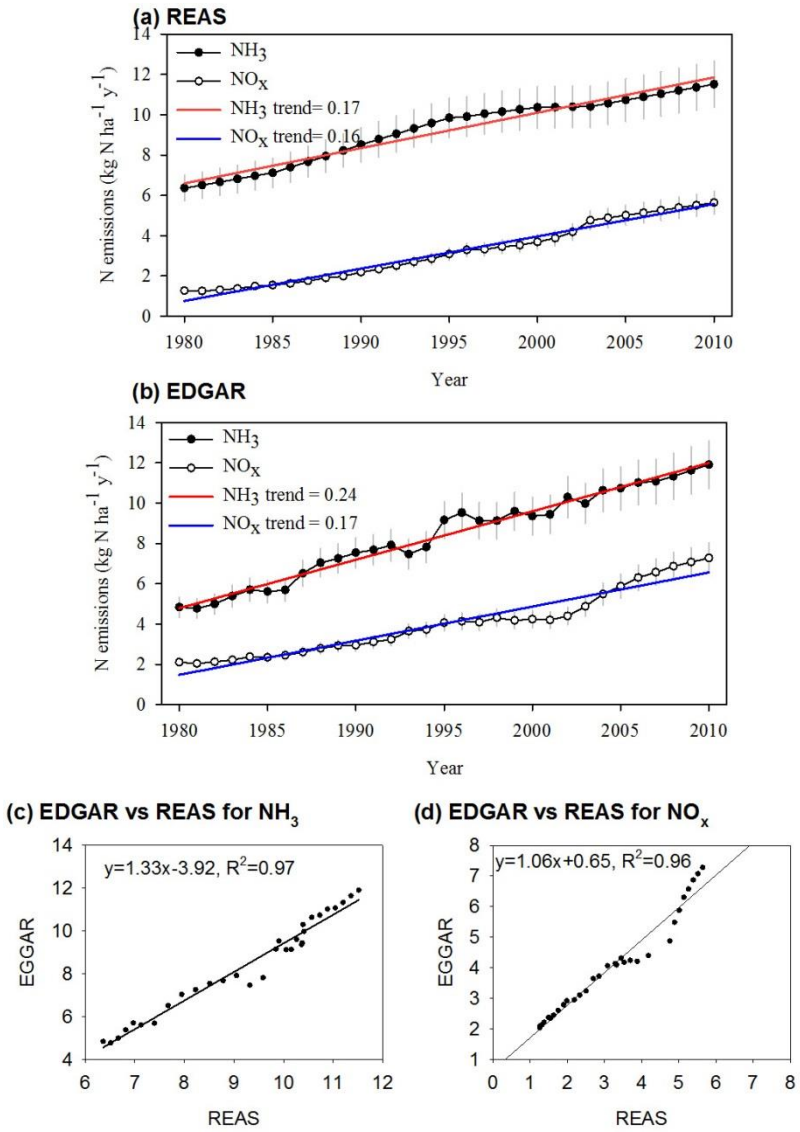

720

721 **Fig. 2**. The NO_2 and NH_3 emissions over China. (a) denotes the NO_2 and NH_3 emissions over China from 1980 to 2010 from
722 REAS, (b) represents the NO_2 and NH_3 emissions over China from 1980 to 2010 from EDGAR, (c) demonstrates the relationship
723 of NO_2 emissions over China from REAS and EDGAR and (d) shows the relationship of NH_3 emissions over China from REAS
724 and EDGAR.

725

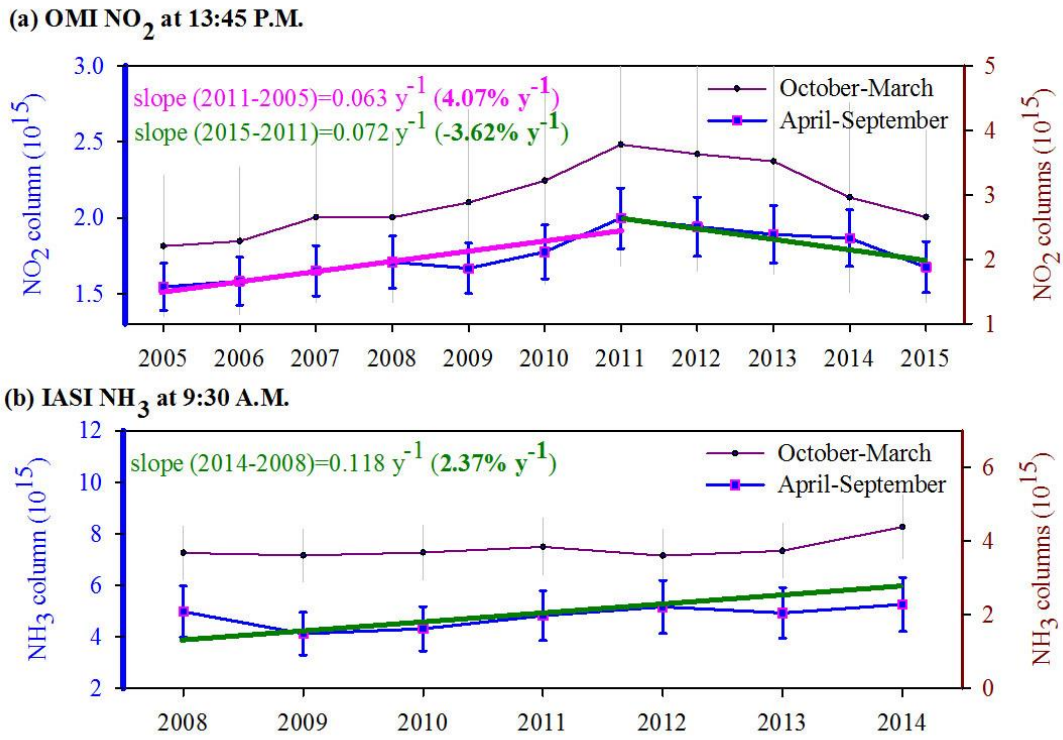

Fig. 3. Time series of average OMI NO_2 and IASI NH_3 columns over China during warm months (April-September) and cold months (October-March). The time period of NO_2 columns was from 2005 to 2015, while the timespan of NH_3 columns was from 2008 to 2015 over China. The associated mean error for each period is presented here as error bars. The percent increase or decrease rate (%) was the long term mean calculated by $100\times(\frac{Y_2-Y_1}{Y_1}+\frac{Y_3-Y_2}{Y_2}+\cdots+\frac{Y_{n+1}-Y_n}{Y_n})\times\frac{1}{n}$.

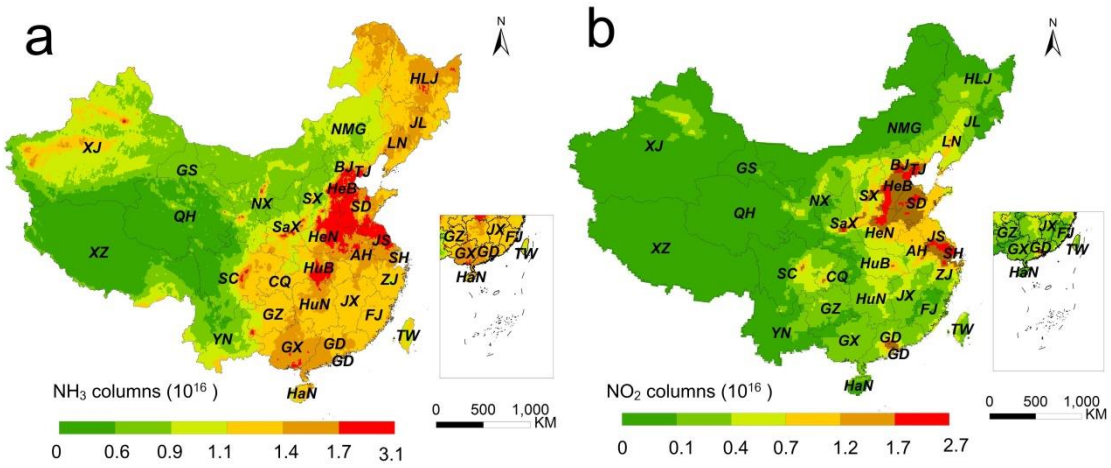

Fig. 4. Spatial distribution of the annual NH_3 (a) and NO_2 (b) columns (molecules cm^{-2} $year^{-1}$). The successfully full provincial names are Beijing (BJ), Tianjin (TJ), Hebei (HeB), Shandong (SD), Shanxi (SX), Henan (HeN), Shaanxi (SaX), Liaoning (LN), Jilin (JL), Heilongjiang (HLJ), Neimenggu (NMG), Gansu (GS), Ningxia (NX), Xinjiang (XJ), Shanghai (SH), Jiangsu (JS), Zhejiang (ZJ), Anhui (AH), Hubei (HuB), Hunan (HuN), Jiangxi (JX), Fujian (FJ), Guangdong (GD), Hainan (HaN), Yunnan (YN), Guizhou (GZ), Chongqing (CQ), Sichuan (SC), Guangxi (GX), Xizang (XZ) and Qinghai (QH).

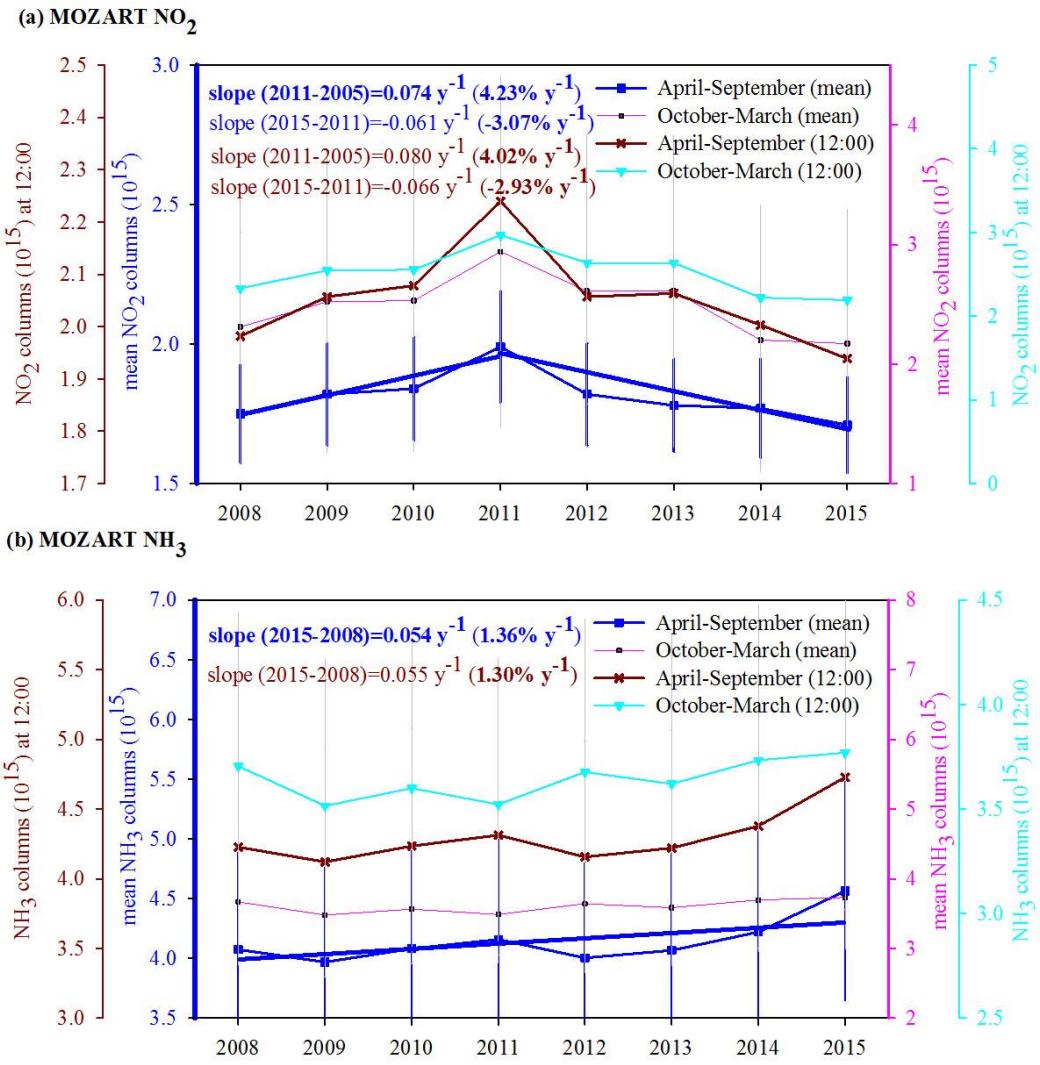

739

740 **Fig. 5.** Time series of MOZART NO_2 and NH_3 columns over China during average warm months (April-September) and cold
741 months (October-March) from 2008 to 2015. The mean columns were calculated by averaging the columns at 00, 6, 12 and 18 h.
742 The associated mean error for each period is presented here as error bars.

743

744